Numerical Modeling of the Spatial Profiles of High-order Harmonics

Muffett, J. E; Wahlström, Claes-Göran; Hutchinson, M. H. R

Published in:
Journal of Physics B: Atomic, Molecular and Optical Physics

DOI:
10.1088/0953-4075/27/23/013

1994

Numerical modelling of the spatial profiles of high-order harmonics

1994 J. Phys. B: At. Mol. Opt. Phys. 27 5693

(http://iopscience.iop.org/0953-4075/27/23/013)

J. Phys. B: At. Mol. Opt. Phys. 27 (1994) 5693–5706. Printed in the UK

Numerical modelling of the spatial profiles of high-order harmonics

J E Muffett†, C-G Wahlström‡ and M H R Hutchinson†

† The Blackett Laboratory, Imperial College, London SW7 2BZ, UK
‡ Department of Physics, Lund Institute of Technology, S-221 00 Lund, Sweden

Received 24 March 1994, in final form 15 September 1994

Abstract. The far-field spatial distributions of high-order harmonics in an ionized medium have been investigated using a computer model that includes both the single atom effects and the collective effects of the medium. The results show that depletion of the non-linear medium due to ionization and radial phase variations across the gas jet cause broadening and complicated structures in the far-field spatial distributions. These phase variations are due to three factors: focusing, ionization, i.e. depletion of the non-linear medium and electron dispersion, and intensity-dependent phase variations of the atomic dipoles.

1. Introduction

There have recently been a number of experiments investigating the spatial structures of high-order harmonics. An experiment by Tisch *et al* (1994) using helium at an intensity sufficient for significant ionization showed that in the plateau region up to $q=101$ the harmonics had a much broader, more complicated structure than that predicted by perturbation theory. Under conditions of minimal phase mismatch Peatross and Myerhofer (1994) found that the far-field angular distributions of the harmonics of Ar, Kr and Xe had a narrow central peak with broad shoulders. This was explained by considering an intensity-dependent phase of the emitting atomic dipoles. Salières *et al* (1994) performed an experiment on the spatial profiles of the high-order harmonics generated in Ne and Ar using a short pulse (140 fs) Cr:LiSAF laser. They found that at intensities below saturation the harmonics were emitted in a narrow cone with a divergence dependent on whether the harmonics belong to the cut-off or to the plateau region. In order to be able to numerically model these experiments, the computer model must include several different effects. In this intensity regime, where there is non-negligible ionization, the non-linear interaction is a complicated combination of single atom effects, electron dispersion, depletion of neutrals and focusing conditions. The computer model must also be three-dimensional to be able to properly account for the spread of the ionized region as the laser pulse passes through the medium.

This work utilizes a computer model similar to that employed by L'Huillier *et al.* (1991). The information about the single atom response has been supplied by Rae and Burnett (1993). The model has been used to study numerically the spatial profiles of high-order harmonic generation in order to identify which of the different physical

0953-4075/94/235693+14$19.50

processes is dominant under given experimental conditions. In order to make use of high harmonic radiation in different applications its main features such as the temporal and spatial profiles should be well characterized. The intensity of the harmonic radiation will ultimately be determined by its focusability and pulse length. It is therefore important to study how these properties are affected by different parameters in order to be able to optimize the design of the harmonic generation process for a given application.

2. The model

The focusing geometry and the interaction region in a typical set-up for high-order harmonic generation are shown in figure 1. The laser is focused into a non-linear medium using a lens. The tightness of the focusing is characterized by the confocal parameter, b, which is equal to twice the distance over which the beam doubles its cross section area and is given by $b=\omega_0^2 k$ where ω_0 is the minimum beam waist radius and

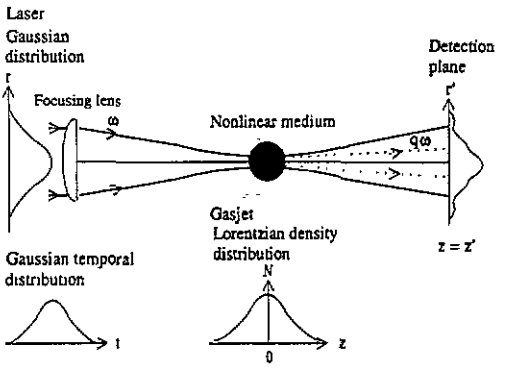

Figure 1. A typical set-up for high-order harmonic generation.

k is the wavevector of the laser. The non-linear medium is usually a gas jet of a noble gas i.e. xenon or helium. The generated harmonic radiation propagates colinearly with the fundamental laser radiation and different harmonic orders are separated by a dispersion element which is usually a grating. Spatially the laser is modelled as a focused Gaussian, and temporally as a Gaussian distribution, though if digitized experimental data are available, e.g. from a streak camera, these can be used to produce a closer agreement with the experiment. The gas jet is modelled as a Lorentzian in the propagation direction, and as a constant in the radial direction. This follows from the fact that the waist of the focused laser beam is normally much narrower than the gas jet; typically the gas jet is 1 mm wide and the diameter of the focus is tens of μm.

The propagation of the electric field, $\boldsymbol{E}$ in an isotropic dielectric medium characterized by polarization, $\boldsymbol{P}$ is described by the inhomogeneous wave equation,

$$\nabla^2 \boldsymbol{E} - \frac{1}{c^2}\frac{\partial^2 \boldsymbol{E}}{\partial t^2} = \mu_0 \frac{\partial^2 \boldsymbol{P}}{\partial t^2}. \tag{1}$$

After taking the Fourier components of $\boldsymbol{E}$ and $\boldsymbol{P}$ at frequency $q\omega$ and assuming that the incident field is linearly polarized the solution of this equation, using the integral

equation method (Bloembergen and Pershan 1962), is

$$E_q(r', t) = \left(\frac{q\omega}{c}\right)^2 \int_V \frac{e^{ik_q R}}{R}[P_q(r, t)]\, dV \tag{2}$$

where the brackets denote the retarded value of P_q and $R = |r' - r|$ is the distance between the volume element dV located at r and the point of observation at r'. This reduces the differential equation to a 3D integral over the volume V of the non-linear medium. The interpretation of this equation is that the electric field at r' is the coherent sum of the dipole radiation generated by P_q in all parts dV of the non-linear medium. After making the paraxial and the far-field approximation, assuming cylindrical symmetry and using a similar method to that employed by L'Huillier *et al* (1992b) the electric field of the qth harmonic in the far field can be written

$$E_q(r', z', t) = \left(\frac{q\omega}{c}\right)^2 \int_{r=0}^{r_{max}} \int_{z=z_{min}}^{z_{max}} \frac{P_q(r, z, t') \exp(-i\int_{-\infty}^{z} \Delta k_q(r, z', t')\, dz'}{z' - z}$$

$$\times J_0\left(\frac{k_q r' r}{z' - z}\right) \exp\left[-ik_q\left(\frac{r'^2 + r^2}{2(z' - z)}\right)\right] 2\pi r\, dr\, dz \tag{3}$$

where t' is the retarded time. It can be seen that this is a diffraction integral of $P_q(r, z, t') \exp(-i\int_{-\infty}^{z} \Delta k_q(r, z', t')\, dz')$, where the phase mismatch is given by

$$\Delta k_q = k_q - qk_1 = \frac{q\omega}{c}\left(n_q - n_1\right). \tag{4}$$

The phase mismatch includes the dispersion of the neutral medium and of the free electrons. Once ionization takes place the electron dispersion dominates. Therefore the dispersion of the ions is ignored. The different frequency components propagate through the non-linear medium at different speeds which causes the harmonic to be out of phase with the laser driving the interaction. Therefore harmonic fields generated at different positions will have different phases and the total harmonic intensity detected will be reduced by the destructive interference. The phase matching also depends on the phase slip due to focusing that occurs between the fundamental and the harmonic waves in travelling through the focus. Wave-mixing and pump depletion are ignored as the pressures and conversion efficiencies are low. In an intense pulse, the ponderomotive force acts to push the electrons away from regions of high intensity, but this is opposed by space-charge forces. From particle-in-a-cell simulations (Rae 1993) the intensity (in W cm^{-2}) has to be roughly the same as the density (in cm^{-3}) before ponderomotive forces start to dominate. For densities of 10^{17} cm^{-3} an intensity of 10^{17} W cm^{-2} would be required which is much higher than the typical intensities of 10^{14} W cm^{-2} considered in the experiments we are modelling. In our model the electrons are hence assumed to remain stationary. The non-linear polarization P_q, is calculated using single atom data obtained with a code written by Rae and Burnett (1993). This code integrates the one-dimensional time-dependent Schrödinger equation. In the non-perturbative regime the polarization is given by L'Huillier *et al* (1991)

$$P_q(r, t) = 2N(r, t) d_q(r, t)\ e^{-iq\phi_{laser}} \tag{5}$$

where $d_q(r, t)$ is the dipole moment and ϕ_{laser} is the phase of the focused laser beam,

$$\phi_{laser}(r, z) = \tan^{-1}\left(\frac{2z}{b}\right) - \frac{2k_1 r^2 z}{b^2 + 4z^2}. \tag{6}$$

The dipole moments are calculated by taking the Fourier transform of the dipole acceleration. This model has an approximate one-dimensional potential given by

$$V(x) = \frac{-1}{\sqrt{1+x^2}}. \tag{7}$$

The photon energy in the model is scaled to give the correct number of photons for ionisation which is 21.03 for helium at 1053 nm. The electric field, E is also scaled using Eberly (1990)

$$\left(\frac{E_{atom}}{E_{model}}\right)^4 = \left(\frac{IP_{atom}}{IP_{model}}\right)^6 \tag{8}$$

where IP_{atom} and IP_{model} are the ionization potentials of the real atom and the model respectively.

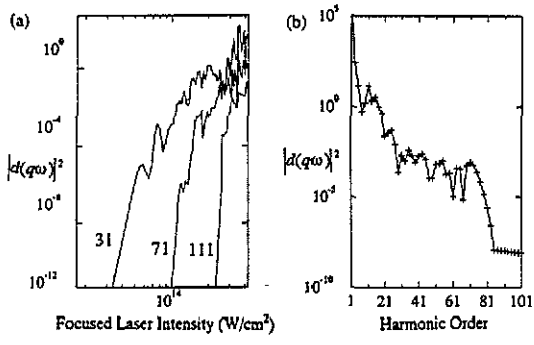

Figure 2. (*a*) Intensity dependence of the 31st, 71st and 111th harmonic dipole moments in helium. (*b*) Harmonic spectrum for the model helium atom at an intensity of 1.7×10^{14} W cm^{-2}.

The variation of the dipole moment with intensity for the 31st, 71st and 111th harmonics in helium is shown in figure 2(*a*). In spite of its simplicity the 1D code gives results which include most of the major features of a typical atom: a steep increase at low intensity followed by a saturation regime with fluctuations. The onset of the saturation regime marks the intensity when a particular harmonic begins to be part of the plateau in the spectrum of the harmonics. This is shown in figure 2(*b*) for helium at an intensity of 1.7×10^{14} W cm^{-2}. It can be seen that the 71st harmonic is just at the edge of the plateau at this intensity which corresponds to the beginning of the saturation regime in figure 2(*a*). The main difference between the model and real atomic potentials is that the dips and peaks associated with the atomic resonances will occur at different intensities. However, it provides useful insight into the general behaviour of the harmonics in the plateau and cut-off regions. The average slope of the dipole moments in the saturation region is about 8. An approximate way of describing these harmonics is as the polarization varying as the 8th power of the laser intensity. However this neglects completely the dips and the fast variation of the dipole phase in this region. The ionization rate can also be obtained from the single atom code; it is a measure of the

decrease of the norm of the wavefunction as the flux is absorbed at the edges of the radial grid during the numerical integration.

3. Results

3.1. Weak-field and approximate strong-field theory

Although lowest-order perturbation theory (LOPT) is inadequate to describe interactions in the strong-field regime it is helpful for further comparisons to summarize the results obtained with this theory and at the same time neglect ionization. The qth harmonic polarization, P_q varies as the qth power of the laser electric field, E_1, i.e. $P_q \propto E_1^q$ and hence the harmonic intensity varies as the qth power of the laser intensity. In the weak-field limit the qth harmonic has the form of a focused Gaussian beam centred at the same point as the fundamental and with the same confocal parameter. The beam waist radius at the focus of the qth harmonic, $\omega_0^{(q)}$ is $q^{1/2}$ times smaller than the corresponding radius of the laser; $\omega_0^{(q)} = \omega_0^{(1)}/q^{1/2}$. Similarly, the far-field distribution is given by

$$I^{(q)}(r', z') \propto \exp\left(\frac{-qk_1 b(r')^2}{2(z')^2}\right) \tag{9}$$

where the $1/e^2$ radius is given by $\omega_1(z')/q^{1/2}$ and $\omega_1(z')$ is the corresponding radius of the fundamental. As the harmonic order increases the width of the far-field profile decreases by $1/q^{1/2}$. The temporal profile will vary as $I^{(1)}(t)^q$ and the $1/e^2$ temporal width will also decrease with order as $1/q^{1/2}$.

The single-atom code shows that once the intensity is high enough to make a particular harmonic part of the plateau the polarization of that harmonic increases more slowly with laser intensity than in the perturbative limit and by a similar rate for different harmonics. From this it follows that an approximate way of writing the polarization in this strong-field regime is $P_q \propto |E_1|^p \exp(iq\phi_{\text{laser}})$ where p is the effective order of non-linearity while the phase term keeps the q-dependence. For a focused Gaussian laser distribution this can be written (L'Huillier *et al* 1992b)

$$P_q(r, z) \propto \frac{1}{(1+4z^2/b^2)^{p/2}} \exp\left(\frac{-pk_1 r^2 b}{b^2+4z^2}\right) \exp\left(-iq\left(\tan^{-1}(2z/b) - \frac{2k_1 r^2 z}{b^2+4z^2}\right)\right). \tag{10}$$

For helium we found from the numerical solution of the time-dependent Schrödinger equation that, on average, the polarization increases approximately as the 8th power of the intensity so in this case $p = 8$. The qth harmonic in this approximate strong-field regime and with loose focusing has the form of a focused Gaussian beam centred at the same point as the fundamental but with the confocal parameter increased by a factor q/p. The beam waise radius is therefore increased compared to LOPT by the factor $(q/p)^{1/2}$. The far-field distribution is given by

$$I^{(q)}(r', z') \propto \exp\left(\frac{-k_1 b(r')^2 q\left(\frac{q}{p}\right)}{2(z')^2}\right). \tag{11}$$

In this case the width of the far-field profile is narrower than in the perturbative case by a factor, $(q/p)^{1/2}$, the same factor as the beam waist became wider. The temporal profile will vary as $I(t)^p$ and the $1/e^2$ temporal width is $(q/p)^{1/2}$ times larger than in the perturbative case.

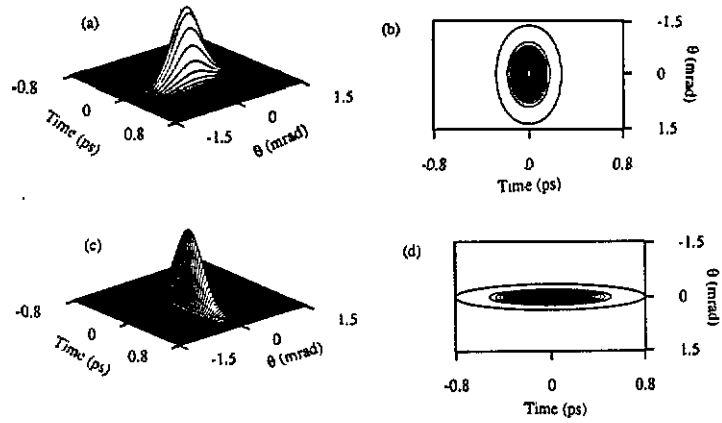

Figure 3. (*a*) and (*b*) show the 3D representation and contour plot of the 71st harmonic in helium at an intensity below ionization in the perturbative limit, $P_q \propto E^{71}$. (*c*) and (*d*) were calculated for the strong-field regime, $P_q \propto |E|^8$.

The variation at an intensity below ionization of the 71st harmonic in helium in space and time is shown in figure 3. Figure (3)(*a*) shows the 3D representation of the far-field spatial and temporal profiles of the 71st harmonic calculated from perturbation theory and figure 3(*b*) is the corresponding contour plot with the contour levels set at constant intervals. Figures 3(*c*) and (*d*) are the same graphs calculated in the strong-field regime with $p=8$. Comparison of the widths in the weak and strong field cases gives two simple relations: the temporal profile is $(q/p)^{1/2}$ (≈ 3) times wider in the strong-field case, while the far-field spatial profile is narrower by the same factor. As ionization of the medium was not considered at this stage the temporal profile in both cases can be seen to be symmetric about the $t=0$ position which represents the peak of the incoming pulse.

3.2 Focusing

The far-field spatial profile of the 71st harmonic at an intensity well below the saturation intensity for ionization but in the strong-field regime, for three different focusing conditions is shown in figure 4(*a*). The results were obtained using the approximate strong field theory, not results from the single atom code. The confocal parameter, b, is set at 10 mm and the FWHM of the gas jet, L, is varied. This is equivalent to varying b for a fixed gas jet width, as would normally be done when the focusing effects are being investigated experimentally, as it is the quantity L/b which is important. In the loose focusing limit, $L/b \ll 1$, the far-field profile is described by a Gaussian distribution but as the focusing becomes tighter the spatial profile becomes distorted and develops ring. The expressions for the radial variation of the amplitude and the phase of the polarization are $\exp(-pk_1 r^2 b/(b^2+4z^2))$ and $\exp(iq2k_1 r^2 z/(b^2+4z^2))$ respectively. In the perturbative limit both of these quanties vary to the qth power and the amplitude falls off in the radial direction before there is much phase oscillation. However, in the strong-field case, the polarization amplitude falls off less rapidly and there are more phase oscillations in the polarization and hence in the harmonic electric field (L'Huillier *et al* 1992a). It is these radial phase oscillations in the focal region that cause the distortion in the far-field intensity profile. From the phase term it can be seen that both increasing

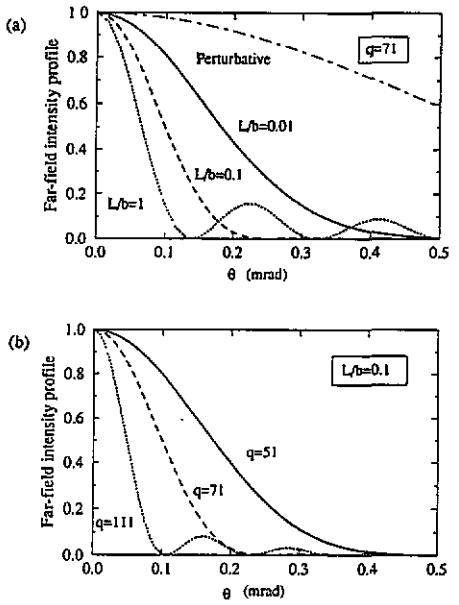

Figure 4. The far-field profile in the strong-field regime with no ionization. (*a*) depicts three focusing regimes: loose ($L/b=0.01$, solid curve), intermediate ($L/b=0.1$, dashed curve) and tight focusing ($L/b=1$, dotted curve) for the 71st harmonic. (*b*) shows the effect of varying the harmonic order in one focusing regime ($L/b=0.1$), $q=51$ (solid curve), $q=71$ (dashed curve) and $q=111$ (dotted curve).

q and decreasing b (for a particular L) cause the oscillation frequency to increase and hence the far-field distortion to intensify. The effect of increasing the harmonic order for a particular set of focusing conditions is shown in figure 4(*b*). It can be seen that the focusing effects become more important as higher orders are reached. In order to minimize focusing distortions, small ratios of L/b should be used and as the harmonic order is increased the ratio of L/b should be decreased accordingly. Simulating the experimental conditions used in Tisch *et al* (1994) ($L=1$ mm and $b=20$ mm) the far-field profiles of the harmonics considered ($q=69$ to $q=111$) are slightly narrowed as compared to the loose focusing regime ($L/b\ll 1$) where b was kept constant and L was decreased accordingly, but the ring structure observed in the experiment is not reproduced in this calculation.

The effect of radial phase variations due to focusing of the laser beam can be readily demonstrated by noting that, in the loose focusing regime with a very thin gas jet, the far-field profile is approximately given by the Hankel transform of the harmonic electric field distribution at the focus. This transform reproduces the results of the 3D harmonics integral in section 2, in the loose focusing limit for the weak and strong-field regimes. In the perturbative case (figure 5(*a*)) the harmonic profile at the focus will be described by a Gaussian distribution taken to the qth power which, when transformed to the far field, gives a Gaussian distribution with a width equal to $1/q^{1/2}$ times the width of the fundamental. In the strong-field regime (figure 5(*b*)) the qth harmonic profile at the focus is broader than in the weak field by a ratio $(q/p)^{1/2}$ and hence the far-field profile is narrower than in the perturbative case by the same factor. If, on the other hand, the Gaussian laser beam has radial phase structures, the far-field profile of the harmonics

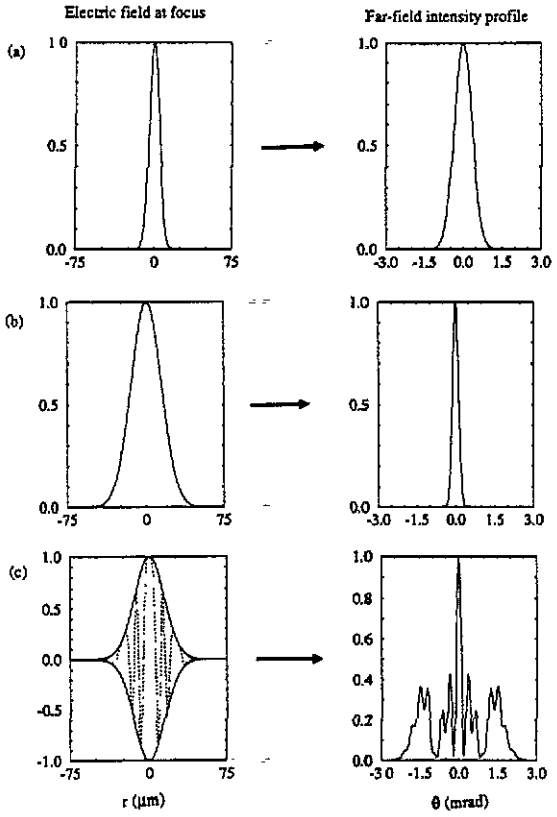

Figure 5. The electric field distributions of the 71st harmonic at the focus and the far-field intensity pattern calculated by taking the Fresnel-Bessel transform. (*a*) represents the perturbative regime, $P_q \propto E^{71}$, and (*b*) the strong-field regime, $P_q \propto |E|^3$. (*c*) shows the strong-field regime with an additional cosinusoidal phase factor across the focus. The real part of the electric field showing the phase variation (dotted curve) and the modulus of the electric field (solid curve) at the focus are shown.

will be broadened. For example, modifying the phase of the Gaussian beam by multiplication by a cosine function of r, gives the far-field profiles shown in figure 5(*c*). Once this phase variation is included the far-field profile is no longer a narrow Gaussian but the energy is spread out into a complicated wing structure, similar to that reported by Tisch *et al* (1994).

3.3 Ionization and electron dispersion

In order to study the effect that ionization has on the temporal and far-field spatial profile of high-order harmonics in the strong-field regime, calculations were done for different degrees of ionization. In this part of our study we calculated the space and time dependent ionization using a simple rate equation for ionization and assuming a saturation intensity for ionization of He of 2.8×10^{14} W cm^{-2}. The degree of ionization at the focus for two peak intensities, with a laser pulse length of 1.3 ps, is shown in

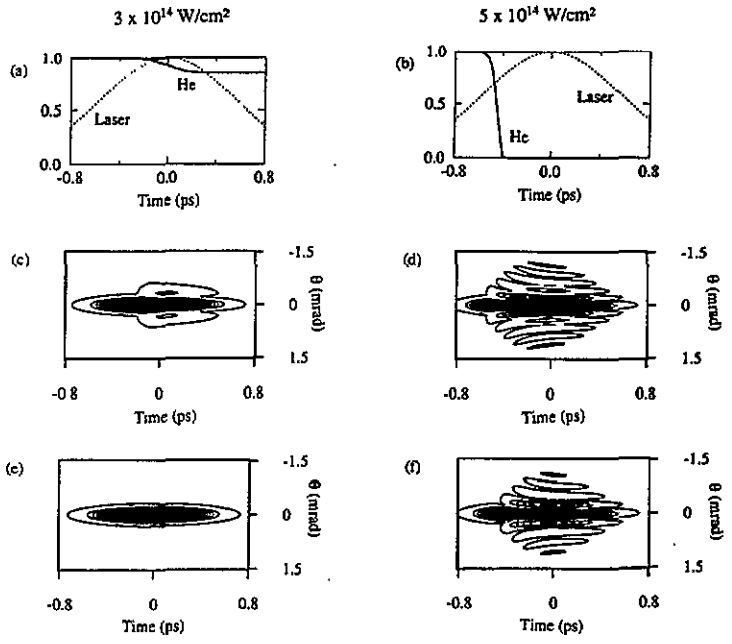

Figure 6. Contour plots for the 71st harmonic in helium at intensities 3×10^{14} W cm^{-2} and 5×10^{14} W cm^{-2}. (*a*) and (*b*) show the degree of ionization at the focus, calculated from the experimental value for the saturation intensity for ionization. In (*c*) and (*d*) electron dispersion is included while in (*e*) and (*f*) the electron dispersion is switched off.

figures 6(*a*) and (*b*). At 3×10^{14} W cm^{-2} there is 15% ionization by the end of the pulse, but at 5×10^{14} W cm^{-2} there is 100% ionization 0.4 ps before the peak of the laser pulse.

For both intensities contour plots of the far-field profiles of the 71st harmonic are shown with and without electron dispersion: at 3×10^{14} W cm^{-2} in figures 6(*c*) and 6(*e*) and at 5×10^{14} W cm^{-2} in figures 6(*d*) and 6(*f*). Once ionization has occurred rings begin to develop. As the intensity increases further more rings appear more closely together. Once the intensity of the input pulse has decreased sufficiently for no more ionization to occur the shape of the far-field distribution remains the same whilst the intensity of the profile diminishes. Before ionization, the far-field spatial profile is described by a Gaussian distribution because it is the Fourier transform of a Gaussian distribution at the focus, but as ionization occurs the focal region becomes depleted and the harmonics are generated further out in the wings of the gas jet. The shape of the region within the focal volume where the harmonics are produced now has the appearance of a Gaussian with the centre missing. The 2D Fourier transform of this shape has rings and as the depleted central region spreads out further radially more rings develop in the far field that are more closely spaced.

In addition to depletion of the non-linear medium there is also the effect of the electron dispersion. The dispersive character of the free electrons generates a large positive phase mismatch which is given by

$$\Delta k_q^{\mathrm{elec}}(r)=\frac{\omega_p^2(r)(q^2-1)}{2q\omega c} \tag{12}$$

where the plasma frequency, ω_p, at a given point in space is proportional to the square root of the local electron density.

As the intensity increases and becomes sufficient for ionization, the gas will first be ionized mainly close to the optical axis. This leads to a radial variation in the density of free electrons and hence a radially varying phase mismatch. In the expression for the harmonic electric field there is a term $\exp(-i\int_{-\infty}^{z}\Delta k_q(r, z', t')\,dz')$. The phase mismatch due to the free electrons is included in this term and hence the harmonic field across the medium will have a radial phase variation. This will then cause the far-field spatial distribution to spread out and develop rings, compare figures 6(*c*) and 6(*e*).

An important result from the experiment by Tisch *et al* (1994) was that the harmonics in the plateau had a broad complicated structure whilst the harmonics beyond the cut-off were much narrower and close to the perturbative limit. Under these experimental conditions, as discussed aboye, the focusing effects are minimal while the electron dispersion has the dominant effect on the far-field spatial profile. As the polarization for the harmonics in the plateau increases more slowly with intensity than the harmonics in the cut-off region, the radial extent of the volume where they are generated is much broader. The density of electrons and hence the phase mismatch varies significantly over this large region leading to large phase changes for these harmonics. The harmonics in the cut-off region, however, are generated in a significantly smaller volume near the optical axis and there is less phase variation from the electrons.

The divergence of the harmonics in the far field will also be influenced by the defocusing of the laser beam propagating through the region with radial electron density gradients in the focal volume. However, the change in the near-field distribution of the fundamental beam has been shown to be small under similar conditions and is therefore neglected in this work (L'Huillier *et al* 1992a).

When ionization is included and the peak intensity considered is comparable to the saturation intensity for ionization or higher, the peak of the temporal profiles of the harmonics will occur before the peak of the laser pulse. Further, its shape deviates from a smooth Gaussian distribution to a more uneven profile which is not necessarily symmetric. At low laser intensities the harmonic temporal intensity profile increases as $I(t)^q$. Once the intensity is high enough for ionization the central region of the gas jet becomes ionized and free electrons are produced. As the intensity increases further the ionization spreads out both radially and along the propagation axis. At this state, if it is assumed that the ions are not contributing, the harmonics are being produced only in the wings of the gas jet. In the recent experiment by Starczewski *et al* (1994) good agreement was found between the model and the experiment for the shift of the peak of the harmonic when both depletion of the neutral gas and electron dispersion were included.

3.4. Intensity-dependent phases of the atomic dipoles

By using in the calculation of the non-linear polarization atomic data obtained by numerically solving the time-dependent Schrödinger equation, two effects are added that were not included in the strong-field approximate model above. Firstly there are resonant dips and peaks of the atomic dipole amplitude and secondly there are intensity-dependent phase variations of the atomic dipoles in the saturation region. Each harmonic will come into the plateau region at a particular intensity and have individual resonant features. As the focused intensity in the gas jet varies in time and space, different parts of the gas jet will show different resonant enhancement. A harmonic in the plateau region will have a fast phase variation across the focal region, whereas a harmonic beyond the cut-off will not have reached sufficient intensity to have much

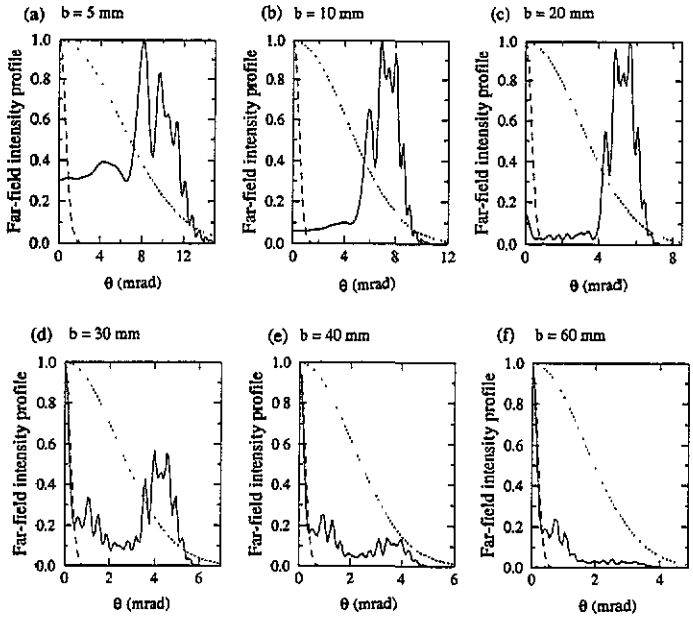

Figure 7. The 91st harmonic in helium (solid curve) for a range of confocal parameters from $b = 5$ mm (a) to $b = 60$ mm (f). The ionization and the harmonic dipole moments are calculated using the 1D code at an intensity of 2.6×10^{14} W cm^{-2}. The perturbative profile (dashed curve) and the laser profile (dotted curve) are also shown. Note the change in scale.

atomic dipole phase variation and will therefore have little phase variation across the focus. This will cause the harmonics in the plateau to have a broadened far-field spatial structure while the harmonics in the cut-off region remain narrow.

In an experiment where the intensity is high enough for significant ionization, all the different effects described above will take part: radial phaseshifts due to focusing, electron dispersion, depletion of the non-linear medium and the effects of intensity-dependent atomic dipole phases. The different effects will dominate under different conditions. In figure 7 the far-field spatial profile of the 91st harmonic in helium is depicted for a range of confocal parameters. The intensity considered is sufficient for significant ionization and the atomic dipole moments from the single atom code are included. At this intensity the 91st harmonic is in the plateau region. As the confocal parameter increases and the focusing effects become less important the wings in the profile become smaller and the energy is drawn back into the centre of the profile causing it to become narrower. (Note the change in scale for the different focusing cases in the figure.) The 91st harmonic is further investigated at two different confocal parameters: $b = 10$ mm and $b = 30$ mm in figure 8. At first all the different effects are included as in figure 7 (see figure 8 (solid curves)). In figures 8(a) and (b) the electron dispersion is switched off (dashed curves) and it can be seen that the electron dispersion is important mainly in the looser focusing case where it contributes significantly to the wing structure. By increasing the pressure from 5 to 20 Torr the number of electrons is increased which causes the wing to increase in size at $b = 30$ mm but has only little effect at $b = 10$ mm. In figures 8(c) and (d) the effect of using only the absolute value of the polarization, not its phase, in the calculation is illustrated (dashed curve). This

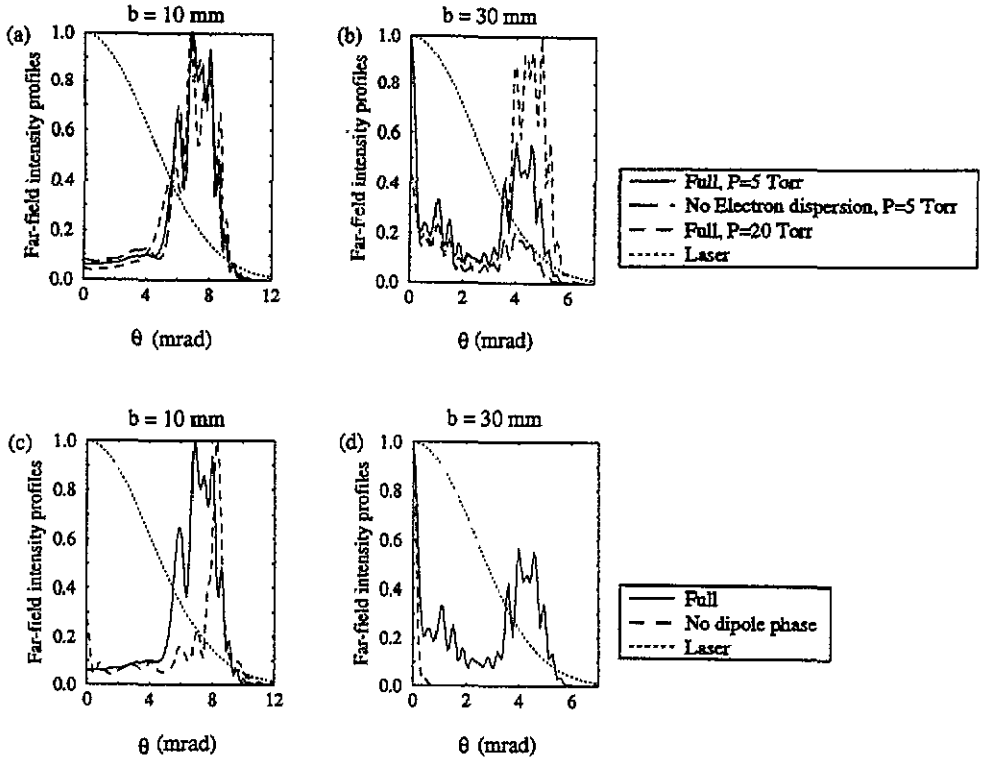

Figure 8. The effect of electron dispersion and atomic dipole phase on the 91st harmonic in helium, at the same intensity as in figure 7. Each case is shown at two confocal parameters: $b = 10$ mm and $b = 30$ mm. The solid curve in all four graphs has all the different effects included. In (*a*) and (*b*) electron dispersion is switched off (dashed curve) and in (*c*) and (*d*) the atomic dipole phase is switched off (dashed curve). Note the change in scale between the two focusing casess.

causes a slight reduction in the energy of the wing at $b = 10$ mm but at $b = 30$ mm removing the phase causes the wing to disappear completely. At small confocal parameters the focusing effects dominate and dictate the shape of the far-field profiles whereas at longer confocal parameters both electron dispersion and the intensity-dependent phases of the atomic dipoles influence the shape of the profiles.

4. Discussion and conclusion

We have investigated numerically the relative role of different parameters influencing the far-field spatial profiles of high-order harmonics. The methods and the approximations used were: the single-atom response to the intense laser field was calculated in two different ways. When investigating the effects of focusing, ionization and of electron dispersion, we used an approximate strong-field model for the dipole moment and a rate equation for ionization. When investigating the effect of the intensity-dependent phases of the atomic dipoles, on the other hand, we used single-atom data from a code which solves the one-dimensional Schrödinger equation. In all cases the propagation effects were calculated using a propagation code based on the slowly varying envelope and the far-field approximation. The laser was assumed to be linearly polarized and

described by lowest order focused Gaussian beam. Pump depletion and higher order, indirect processes were neglected. Axial symmetry was assumed and the photoelectrons were assumed to remain stationary during the laser pulse.

The results show that the broadening and the development of rings in the far-field spatial profiles of high-order harmonics is due to radial variations in the focal region, and in the case of ionization to the depletion of the non-linear medium close to the optical axis. The phase variations are due to the following factors. Firstly a geometrical effect due to the focusing: as the harmonic order increases or the confocal parameter decreases for a particular length of the non-linear medium this effect becomes more important. Secondly ionization, i.e. electron dispersion of the non-linear medium. As the harmonic order or the density of free electrons increases the effect of the electron dispersion increases. The number of free electrons can be increased both by going to higher intensities and hence ionizing a larger volume of atoms or by increasing the pressure of the gas. Third and lastly the intensity-dependent phases of the atomic dipoles: in the saturation regime there is a lot of phase variation due to intensity-dependent resonances but this effect is only of importance for the harmonics in the plateau region. Depletion of the medium and the different sources of radial phase variations are of different relative importance under different experimental conditions.

In many applications the ability to focus the XUV radiation is essential, and hence a smooth spatial profile is desired. The above findings can be used to guide the design of the harmonic generation process in order to optimize the characteristics of the spatial profile for a given harmonic order and a given laser-pulse energy: the focusing should be made as loose as possible as to make the desired harmonic order be in the cut-off region. Loose focusing minimizes the influence of focusing, and the corresponding reduction in intensity keeps the amount of ionization as low as possible. Being in the cut-off region, the influences of the intensity-dependent phases of the atomic dipoles are kept at their minimum. Making the focusing looser reduces the intensity. The total number of harmonic photons, however, is at least partly compensated by the increase in focal cross section and hence by the number of atoms coherently contributing to the macroscopic signal.

Acknowledgments

We wish to thank K Burnett and S Rae for generously providing us with unpublished data from their one-dimensional model calculations. We also thank A L'Huillier for helpful discussions. Financial support by the Science and Engineering Research Council (SERC) and from the Swedish National Science Research Council is gratefully acknowledged.

References

Bloembergen N and Pershan P S 1962 *Phys. Rev.* A **128** 606

Eberly J H 1990 *Phys. Rev.* A **42** 5750

L'Huillier A, Balcou P, Candel S, Schafer K J and Kulander K C 1992a *Phys Rev.* A **46** 2778

L'Huillier A, Lompré L-A, Mainfray G and Manus C 1992b *Atoms in Intense Laser Fields* ed M Gavrila (San Diego CA: Academic)

L'Huillier A, Schafer K J and Kulander K C 1991 *J. Phys B: At. Mol. Opt. Phys.* **24** 3315

Peatross J and Meyerhofer D D 1994 *Proc. 6th Int. Conf. on Multiphoton Processes* (*Quebec, 1993*) ed D K Evans and S L Chin (Singapore: World Scientific)
Rae S C 1993 *Private communication*
Rae S C and Burnett K 1993 *Phys. Rev.* A **48** 2490
Salières P, Ditmire T, Budil K S, Perry M D and L'Huillier A 1994 *J. Phys. B: At. Mol. Opt. Phys.* **27** L217
Starczewski T, Larsson J, Wahlström C-G, Tisch J W G, Smith R A, Muffett J E and Hutchinson M H R 1994 *J. Phys. B: At. Mol. Opt. Phys.* **27** 3291
Tisch J G W, Smith R A, Ciarrocca M, Muffett J E, Marangos J P and Hutchinson M H R 1994 *Phys. Rev.* A **49** 28